

Chapter 6

Cooling in the Circularly Polarized Optical Dipole Trap

6.1 Motivation

Cooling of atoms in a trap using completely optical techniques is an important pursuit of atomic physicists. Optical traps offer rapid control and tight confinement. Optical cooling techniques allow the cooling process to be decoupled from the thermal collisional process, allowing very low temperatures to be achieved while minimizing potentially lossy collisions. A circularly-polarized dipole trap offers a variety of non-degenerate states in which to work, much like a magnetic trap does. Thus many cooling mechanisms previously available only in magnetic traps are available in the circular FORT, and can be implemented optically.

Many schemes exist to cool atoms in red-detuned optical dipole potentials. Evaporative cooling via relaxation of the potential has been used to reach temperatures of $4 \mu\text{K}$ [76], but so-called run-away evaporation was not possible in this scheme because the density of atoms decreases as the potential increases. Raman cooling has also been demonstrated in a dipole trap formed with YAG lasers [91].

Many techniques are employed in optical lattices as well. They include Raman cooling, evaporative cooling, adiabatic expansion, sideband and degenerate sideband cooling [92, 93]. However, optical lattices can be difficult to construct and leave atoms in many different potential wells instead of the same potential well.

Sisyphus cooling refers to any cooling process in which an atom dissipates kinetic energy by physically moving into a region of space in which it loses kinetic energy to potential energy, then changes its internal state to one with smaller potential energy before it leaves the elevated potential. In this way, the atom can be described as continually rolling up hill, much like the mythical Greek Sisyphus was forced to push a boulder eternally uphill. Many different types of Sisyphus cooling exist. It is an essential part of polarization-gradient cooling, which manifests itself as the sub-Doppler cooling mechanism in MOTs [12, 13]. In addition, gravitational Sisyphus cooling [45] employed the Sisyphus cooling concept to two potentials with nearly the same curvature, but displaced from one another. Evanescent wave cooling [94, 95] employs the mechanism as atoms bounce off an evanescent wave atom mirror. Sisyphus cooling is in general much more efficient than Doppler cooling, because a huge fraction of an atom's total energy can be carried away for the cost of 1 recoil photon. The ratio of the potential energies of the two internal states involved sets the amount of energy that can

be extracted in an event. A Sisyphus cooling mechanism clearly presents itself in the circular FORT, where internal energy levels are non-degenerate and separated by much more than the energy of one photon recoil.

Blue Sisyphus cooling (BSC) has been successfully employed to load a dipole trap [69]. Atoms were successfully loaded into linearly polarized YAG traps with temperatures of $2 - 10 \mu\text{K}$. In this way, phase space densities of over 10^{-3} were achieved with 10^4 atoms in an individual potential. The BSC scheme is more similar to the Sisyphus cooling of MOTs, in that the potentials used for cooling are applied by additional lasers, and not supplied by the confining light.

Evaporative cooling is also a very powerful cooling mechanism. By removing the highest energy atoms and allowing the remainder to rethermalize, temperatures of alkali atoms have been reduced many orders of magnitude. In fact, to date it is the only cooling mechanism that remains powerful enough over many orders of magnitude in temperature to achieve Bose Einstein condensation [1]. Evaporative cooling has also been demonstrated in optical dipole potentials, but not without at the same time reducing the spring constant of the trap [76]. Unfortunately, this reduction simultaneously reduces the confinement of the potential, which therefore also reduces the density of the atoms and the collision rate of the atoms. Forced evaporation in magnetic traps, in contrast, can maintain the shape of the potential while removing the fastest atoms from the trap. Such a scheme is possible in the circular FORT just as it is in magnetic traps, and allows for close control of the rate of evaporation, which is necessary for optimization. Forced evaporative cooling has not yet been demonstrated in an optical dipole trap, to our knowledge.

In this chapter, we demonstrate significant cooling in the circular FORT coupled with an increase in phase-space density. The mechanism involved is most likely a combination of forced evaporative cooling and Sisyphus cooling. Preliminary results indicate that these cooling mechanisms are viable. Although these promising results are far from optimized, they point to a powerful new cooling technique for optical dipole traps.

6.2 Theory

6.2.1 Sisyphus Cooling Mechanism

Any Sisyphus cooling mechanism requires that an atom roll up a steep conservative potential gradient, undergo a transition to a different internal state, roll back down a shallower conservative potential, and then be “recycled” to the initial state. This can be accomplished in the circular FORT as shown in Fig. 6.1. Atoms start in the $|F, m_F\rangle = |3, +3\rangle$ state, labeled $|a\rangle$ and described with a potential depth U_a . An atom rolls up the side of the potential, converting kinetic energy to potential. Near the turning point of its oscillation, the atom is driven into an internal state with a smaller AC Stark shift labeled $|b\rangle$ and described with a potential depth U_b . An example with $|b\rangle = |3, +2\rangle$ is shown in Fig. 6.1 (a). The atom then rolls down the shallower potential, in which it gains less kinetic energy than it originally started with. By re-

pumping the atom back to the $|3, +3\rangle$ state at the bottom of the potential, the atom returns to its initial position and internal state with less kinetic energy, closing the cooling cycle. It is then ready to be cooled again. The energy has been carried away by the electro-magnetic fields involved in the transitions.

Many types of transitions can be used to drive this cooling mechanism. Here they are discussed in two categories: the “drive” transitions that excite the atoms to shallower potentials near their turning points, and the “repumping” transitions used to return the atom to the deeper potentials at the bottom of the potential. Figure 6.1 (a) depicts one embodiment of the cooling scheme using a “rf drive”, in which a rf photon drives the atoms into the $|3, +2\rangle$ state, and then the atoms absorb a photon from the circular FORT laser beam to repump them. Figure 6.1 (b) depicts a similar mechanism, where the drive is now an optical two-photon stimulated Raman transition. This transition is induced by an additional “Raman” laser with two frequency components separated by the ground state hyperfine splitting of 3035 MHz plus the difference in their AC Stark shifts at the turning point of the atom. This “microwave drive” can be used in conjunction with the FORT repump described above. Or, an additional repumping laser can be added to provide better state selectivity and more preferentially repump the atoms back to the $|3, +3\rangle$ state to complete the cycle.

The rf and microwave drives each have their advantages and disadvantages. The rf drive is conceptually simpler than the microwave drive as a means to initiate the Sisyphus cooling, since only one photon is required to cause a transition between neighboring m_F states. No additional spontaneous photon scattering is added using the RF drive, whereas the lasers used to create the two-photon Raman transitions also cause additional light scattering. This scattering can cause both simple recoil heating and also heating via the ground state dipole force fluctuations described in Chapter 4. However, one rf cycle generally extracts smaller amounts of energy because the potential energy differences between the levels involved in the rf cycle are generally smaller than those of the microwave cycle.

To implement cooling using the microwave drive, one must maximize the frequency of cooling cycles while minimizing the additional heating rates. Figure 6.2 shows both the spontaneous scattering rate and the resonant Rabi frequency induced by the Raman laser as a function of both the Raman laser frequency and intensity. The resonant Rabi frequency is an important factor in determining the probability that an atom undergoes the two-photon Raman transition. If the atoms were continually resonant with the microwave modulation, they would undergo Rabi flopping between the two states with this frequency. Because the microwave transition actually involves a two-photon stimulated Raman process, $\Omega_{m_f m_i}^{eff}$ depends on the intensity of each frequency component as [96]:

$$\Omega_{m_f m_i}^{eff} = 7.4 \times 10^{13} \frac{\sqrt{I_1 I_2}}{\Delta} f_A(m_f m_i), \quad (6.1)$$

where f_A is a numerical factor depending on the Clebsch-Gordon coefficients between the initial and intermediate states and between the final and intermediate states. For $\Delta m = +1$ transitions, $f_A \approx 0.2$. I_1 and I_2 are the intensities of the two frequency

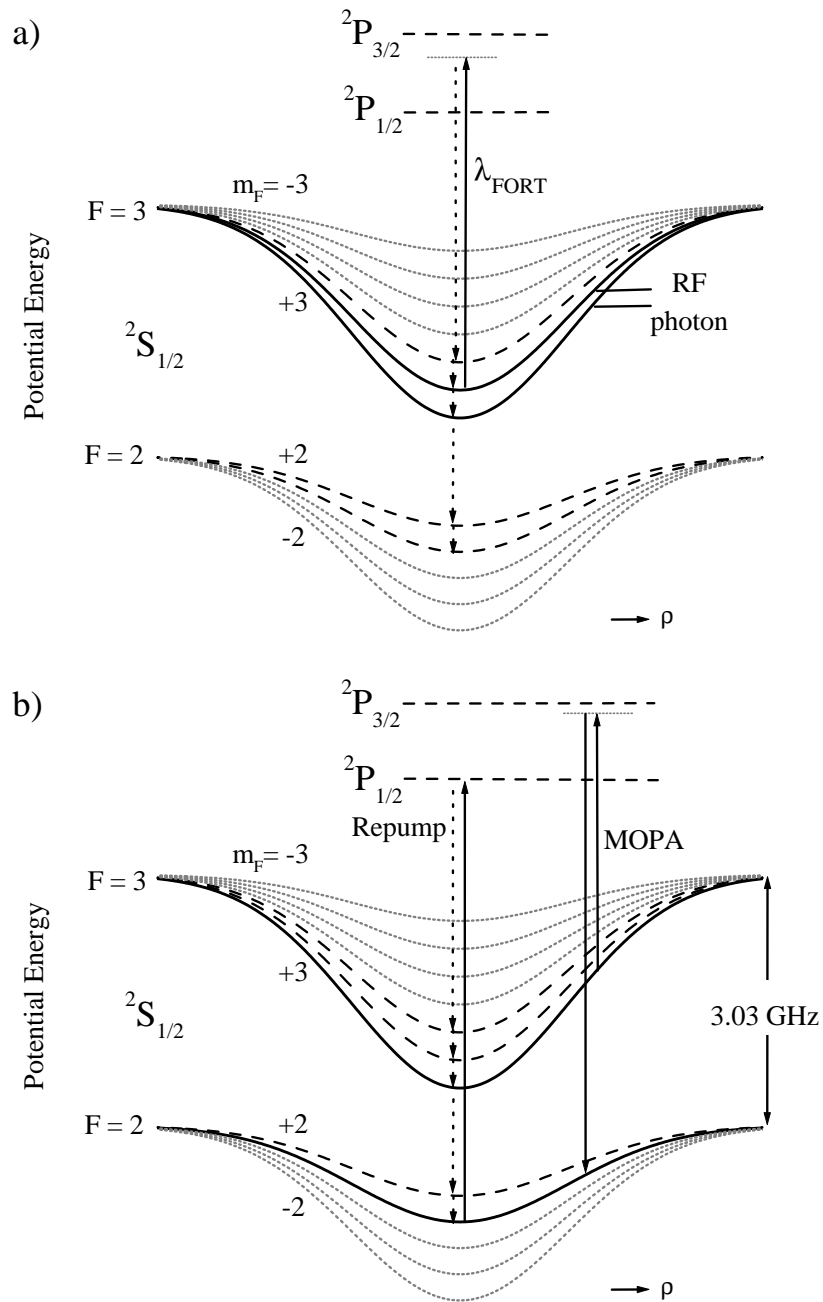


Figure 6.1: Schematic of Sisyphus cooling mechanism utilizing (a) Radio-Frequency transitions to drive the cooling and the FORT spontaneous scattering to repump, and (b) “microwave” two-photon stimulated Raman transitions to drive and an additional laser at 795 nm to repump. The microwave drive shown in (b) will also yield cooling in conjunction with the FORT spontaneous scattering repump shown in (a), as is later demonstrated.

components, in units of mW/cm^2 . Both $\Omega_{m_f m_i}^{eff}$ and the detuning of the laser from resonance with the intermediate state Δ are in units of rad/s .

The effective Rabi frequency changes with laser detuning and intensity, as shown in Fig. 6.2 with a solid line. A dashed line demonstrates the photon scattering rate of atoms in the FORT under the same conditions. In order to use the two-photon Rabi frequencies for cooling, one must find a regime in which the Rabi frequencies are high enough while the heating due to photon scattering is low. To find the optimum detuning and intensity, we must evaluate the drive transition rate.

The rate of atoms making a transition between $|3, +3\rangle$ and $|2, +1\rangle$ is strongly influenced by the presence of the AC Stark shifts. As the atom oscillates in the potential, it sweeps into and out of resonance with the drive field at a fixed microwave frequency. This is exactly analogous to a Landau-Zener transition in which the atom is stationary and the drive frequency is swept from $-\infty$ to ∞ . The more adiabatically (slowly) the frequency is swept, the larger the transfer of population from one state to another in the absence of dephasing (see for example Ref. [97]). This is expressed mathematically by writing the probability P_{LZ} of transferring atoms during one sweep through resonance as [98]

$$P_{LZ} = 1 - \exp(-2\pi\Gamma_{LZ}) \quad (6.2)$$

where the Landau-Zener parameter $\Gamma_{LZ} = \Omega_{eff}^2 (4d\omega_{rf}/dt)^{-1}$. Then $d\omega_{rf}/dt$ is the rate of change of the atom's resonant frequency due to the change in position of the atom with time:

$$\frac{d\omega_{rf}}{dt} = \frac{1}{\hbar} \frac{d}{d\rho} [U(3, +3, \rho) - U(2, +1, \rho)] \frac{d\rho}{dt}. \quad (6.3)$$

$U(F, m_F, \rho)$ is given in Eq. (4.1) and Eq. (4.2). The probability of an atom changing state while oscillating through resonance and back again is $2P_{LZ}(1 - P_{LZ})$.

The velocity of atoms and slope of the potential are continually changing. Therefore, the probability of an atom changing state as it oscillates depends on the frequency of the microwave modulation or analogously on the location in the trap at which the difference in AC Stark shifts between the two states exactly equals the microwave drive frequency. Figure 6.3 shows the probability of an atom changing state, assuming that the microwave frequency is different at each point so as to be resonant with the difference in AC Stark shifts at each point. The maximum probability of a transition is achieved near the turning points of the oscillation, but unfortunately in that case $2P_{LZ}(1 - P_{LZ})$ approaches zero, and no atoms return to the bottom of the well in the $|b\rangle$ state. Within a few Ω_{eff} of the turning point, it is unclear if decoherence will permit transitions to the $|b\rangle$ state to occur at the turning point. If not, the Raman lasers may have to be pulsed on and off so that the transition is no longer adiabatic. The majority of calculations in this Chapter are made assuming a large population transfer at the turning points. Then in Section 6.2.7, modifications brought about by a pulsed scheme will be discussed.

To select the optimum detuning and intensity, it is helpful to examine some general scaling issues. Heating rates are minimized when the spontaneous scattering rate Γ_{sc} is unsaturated, Δ must be large and $\Gamma_{sc} \propto I_t/\Delta^2$ [see Eq. (5.2)]. However, two

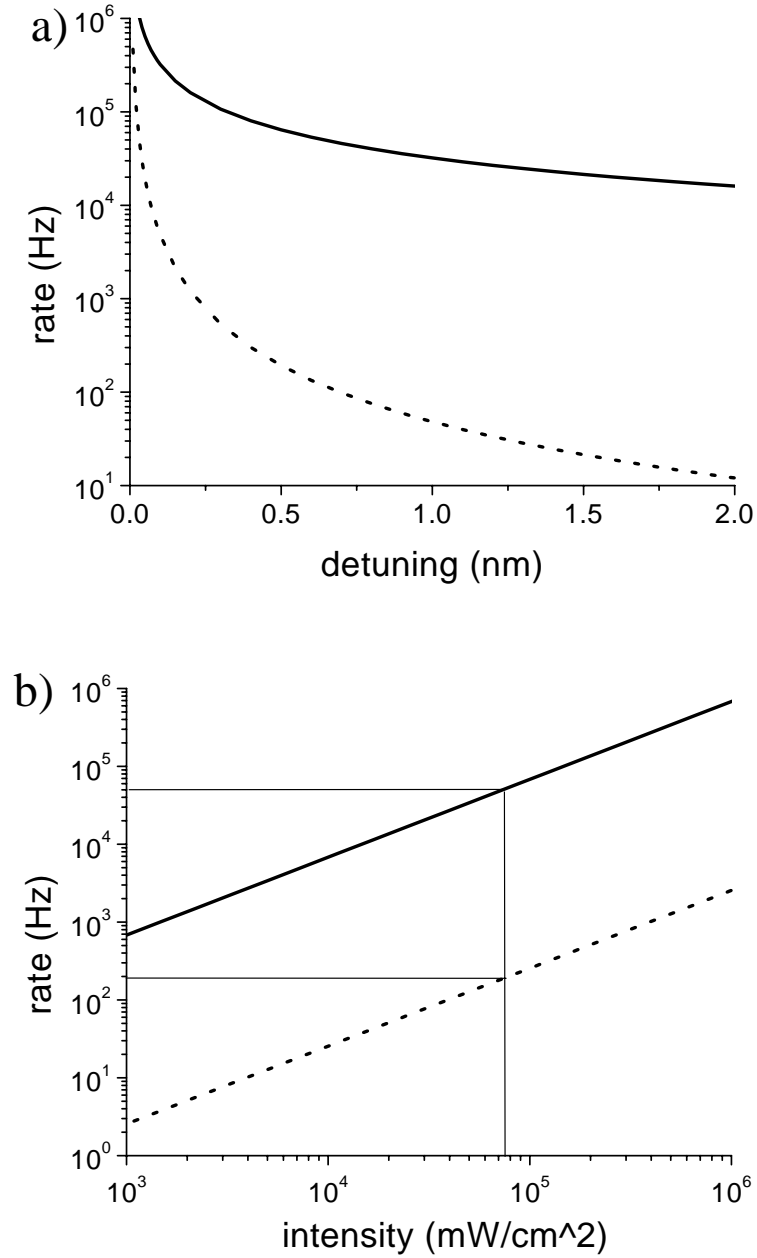


Figure 6.2: Effective Rabi frequency/ (2π) (solid curve) for the two-photon stimulated Raman transition (a) versus the laser detuning for total intensity $I_t = 1.18 \times 10^5$ mW/cm^2 and (b) versus the laser intensity at a fixed detuning of 0.4 nm. Broken curves represent the spontaneous photon scattering rate of atoms in the FORT due to the Raman laser beam. The intensities describe typical experimental conditions. Therefore, $I_t = I_1 + 2I_2$, and the intensity of second frequency component $I_2 = \frac{1}{2}I_1$, where I_t is used to calculate the spontaneous rate and $\sqrt{I_1 I_2} = I_t / \sqrt{8}$ for calculation of the Rabi frequency.

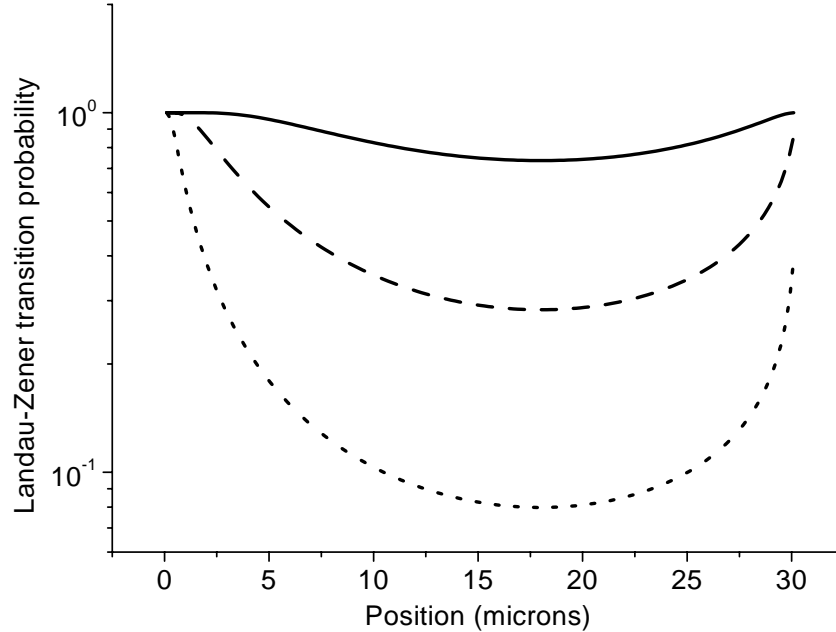


Figure 6.3: Landau-Zener transition probability as a function of position in the circular FORT for 1 atom oscillating in the FORT potential, with a maximum amplitude ρ_{max} of $30 \mu\text{m}$. The microwave frequency is different at each position so as to be resonant with the difference in AC Stark shifts at each point. $I_t = 7.5 \times 10^4 \text{ mW/cm}^2$ (solid), $3.8 \times 10^4 \text{ mW/cm}^2$ (dashed), and $1.9 \times 10^4 \text{ mW/cm}^2$ (dotted).

different regimes must be considered for the Landau-Zener probability. Often, two-photon Raman transitions can be employed with high Rabi frequencies and long interaction times. In this case, the Landau-Zener model no longer applies and atoms can undergo as much as a π -pulse. The time t_π required for a π -pulse scales as $1/\Omega_{eff} \sim \Delta/I_t$, and therefore the ratio of two-photon transition rate to spontaneous scattering rate is proportional to Δ . This scaling also applies to the Landau-Zener transitions when Γ_{LZ} approaches 1. However, when atoms are resonant with the drive frequency for a small fraction of the Rabi oscillation period, Γ_{LZ} is small. Then $P_{LZ} \propto \Omega_{eff}^2 \sim I_t^2/\Delta^2$. Therefore the ratio of Landau-Zener transition rate to spontaneous scattering rate goes with I_t . To demonstrate the Raman transitions, we operate in the small Γ_{LZ} regime. Thus high intensities are critical for observing Raman transitions due to the Raman laser over the background due to spontaneous scattering of the laser.

However, to drive both forced evaporative cooling and Sisyphus cooling, it is important that the microwave frequency stay resonant with atoms near the turning points, where Γ_{LZ} is not small and therefore the first scaling characteristics apply. Thus as atoms are removed from the largest ρ values, the frequency must be decreased in order to interact with atoms at slightly lower energies. The fastest the frequency can be swept and still interact with all atoms is the width of the oscillation every quarter-period of oscillation $\tau_{osc}/4$. The width of the resonance is approximately Ω_{eff} . To cool all the

atoms, the drive frequency must vary at a rate not to exceed $(\Omega_{\text{eff}}/\tau_{\text{osc}})$, and it must interact with atoms at each AC Stark shift. Therefore the duration of the fastest sweep that cools each atom is then the potential depth in MHz divided by the sweep rate in MHz/s. The number of photons spontaneously scattered during this time then scales with ratio of the scattering rate to the Rabi frequency, $\propto 1/\Delta$. Thus the number of photons scattered during an optimized sweep is independent of the Raman laser intensity, assuming there is enough intensity to prevent the Landau-Zener approximation from breaking down.

6.2.2 Repumping with Spontaneous Scattering

Repumping is also an important part of the cooling cycle. For the cycle to be irreversible, it must involve a spontaneous transition. For the cycle to remove any energy, the repumping must occur at smaller differential Stark shifts than the drive transition does. For the circular FORT potentials, the amount of energy extracted per cycle depends on the initial energy E_i , where E_i is the total energy of the atom with respect to the energy of the bottom of the trapping potential U_0 .

$$\frac{\Delta E(E_i, \rho)}{E_i} = \left(1 - \frac{U_b}{U_a}\right) \left(1 - \left(\frac{\rho}{\rho_{\text{max}}}\right)^2\right),$$

The turning point of the atom's oscillation ρ_{max} can be found by solving Eq. 4.1 for ρ :

$$\rho_{\text{max}}(E_i) = w_0 \sqrt{\ln\left(1 - \frac{E_i}{U_0}\right) / -2}. \quad (6.4)$$

The probability that an atom is repumped at a particular ρ depends on the time interval $dt(\rho)$ that it spends at a particular ρ , and $dt(\rho)$ is given by energy conservation

$$dt(\rho) = d\rho \left[\frac{2}{m} U_b (e^{-2\rho_{\text{max}}^2/w_0^2} - e^{-2\rho^2/w_0^2}) \right]^{-\frac{1}{2}},$$

where m is the mass of the Rb atom [99].

Because the detuning and intensity can vary with position, the photon scattering rate Γ_{sc} described in Eq. (5.2) also acquires a ρ dependence. When the FORT light is used as the repump, the detuning Δ is so large that it is essentially uniform across the trap and the rate just depends on the local intensity. In that case,

$$\Gamma_{\text{sc}}^{\text{int}} = G e^{-2\rho^2/w_0^2},$$

where G is an arbitrary constant.

An additional circularly polarized laser tuned close to resonance with the $P_{1/2}$ or $P_{3/2}$ can be added to perform the repumping. Even when it is not focused, selectivity is still provided by the spatial dependence of the detuning provided by the AC Stark shift.

$$\Gamma_{\text{sc}}^{\text{det}}(\rho) = \frac{\Gamma^2}{\Gamma^2 + 4\left[\delta + \frac{U_0}{h}(1 - e^{-2\rho^2/w_0^2})\right]^2}$$

Table 6.1: Repumping from the $|2, +1\rangle$ state. Tabulated are the percent probabilities that an atom decays from the excited state listed across the top to the ground state listed on the left side. These excited states are accessible with a $\Delta m = +1$ transition from the $|2, +1\rangle$ state. Based on calculations by Christopher J. Myatt.

	$5^2P_{3/2}$		$5^2P_{1/2}$	
	$ 3', +2\rangle$	$ 2', +2\rangle$	$ 3', +2\rangle$	$ 2', +2\rangle$
$ 3, +3\rangle$	14	16	11	56
$ 3, +2\rangle$	19	5	15	19
$ 3, +1\rangle$	23	1	19	4
$ 2, +2\rangle$	15	52	19	15
$ 2, +1\rangle$	30	26	37	7

where w_0 is the FORT laser beam waist, the P state linewidth $\Gamma = 6$ MHz, and $\delta =$ detuning of the laser from the AC Stark-shifted atoms at the bottom of the trap. The optimum $\delta = \Gamma/2$ for maximum selectivity.

The average fractional energy change per cooling cycle α can then be computed as a function of the atom's initial energy E_i :

$$\alpha = \left\langle \frac{\Delta E(E_i)}{E_i} \right\rangle = \frac{\int_{\rho=0}^{\rho_{\max}} dt(\rho) \Gamma_{\text{sc}}(\rho) \frac{\Delta E(E_i, \rho)}{E_i}}{\int_{\rho=0}^{\rho_{\max}} dt(\rho) \Gamma_{\text{sc}}(\rho)}, \quad (6.5)$$

where ρ_{\max} is a function of E_i as in Eq. (6.4). The result of this integral as a function of initial energy for both rf and microwave drives, as well as both types of repump transitions, is plotted in Fig. 6.4. From this plot, it is clear that the microwave drive connecting $|3, +3\rangle$ and $|2, +1\rangle$ can remove much more energy per cycle than the rf scheme connecting to $|3, +2\rangle$. In addition, the spatial selectivity of the repumping is not essential for removing energy, as shown by curves 2 and 6. Finally, an optical repumping technique can provide spatial selectivity using detuning. This technique works best when U_b is large compared with the linewidth of the repumping transition, as in curve 3 of Fig. 6.4.

Another large influence on the effectiveness of the repump is the probability that an atom spontaneously decays to the $|3, +3\rangle$ state after being repumped. This depends on quantum numbers of the initial state $|b\rangle$, the polarization of the repumping photon (always σ_+), and the excited state. Examination of the appropriate Clebsch-Gordon coefficients tabulated in Table 6.1 and Table 6.2 reveals some important distinctions between repumping schemes.

The RF cooling scheme excites atoms to the $|3, +2\rangle$ from which they need to be repumped. The circularly polarized FORT laser can do this quite effectively. When it is tuned close to the D_2 transition, 84% of the absorbed photons excite atoms to the $|4', 3\rangle$ state. Of these, Table 6.1 shows that 1/4 decay to the $|3, +3\rangle$ state, while 3/4 decay back to the $|3, +2\rangle$ state in which they started. They then have another chance to make it back to the $|3, +3\rangle$ state while being penalized only 1 photon recoil. Averaging over all transitions, this cycle is 92% closed.

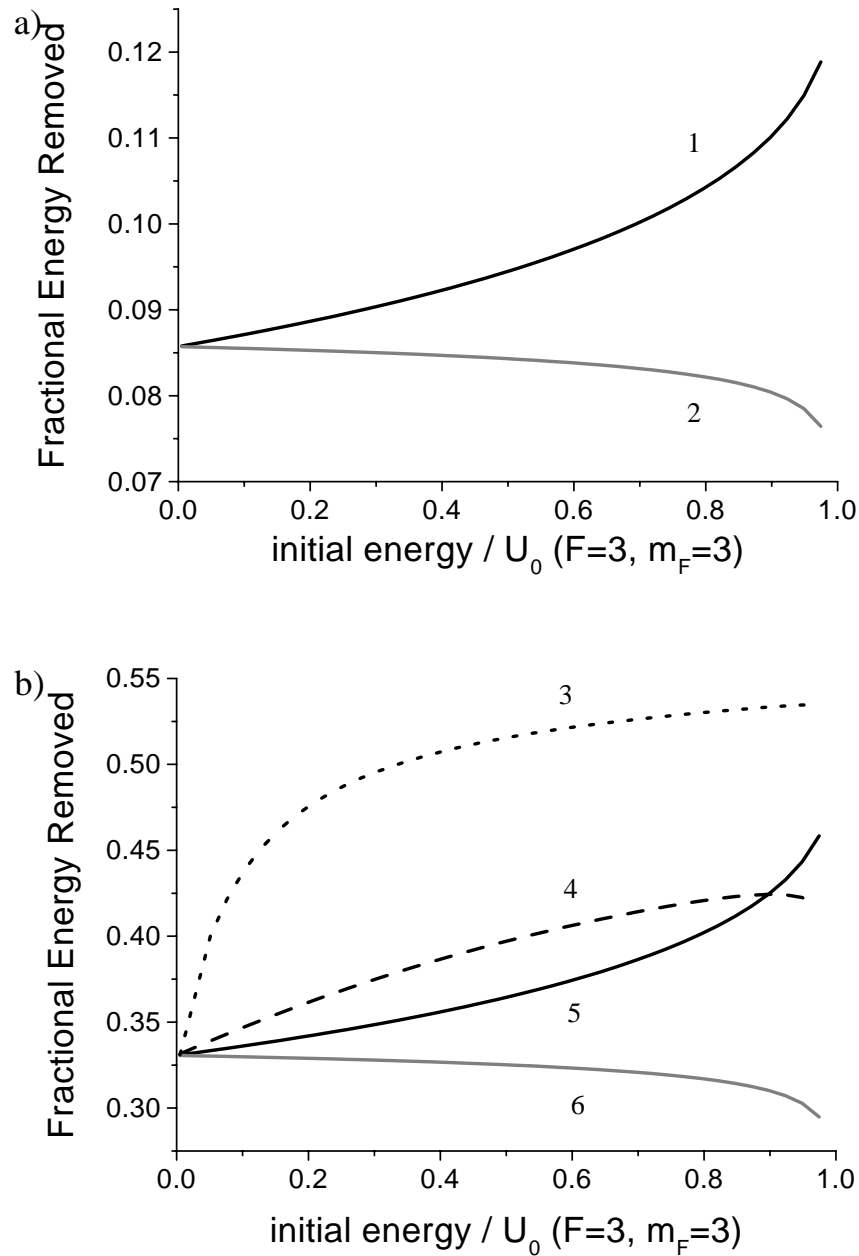


Figure 6.4: Evaluation of Eq. (6.5) as a function of initial energy, for various repumping schemes. **(a)** For $|a\rangle = |3, +3\rangle$ and $|b\rangle = |3, +2\rangle$ as in the rf cooling scheme depicted in Fig. 6.1 (a). **(b)** shows the cooling efficiency for $|a\rangle = |3, +3\rangle$ and $|b\rangle = |2, +1\rangle$ the scheme depicted in Fig. 6.1 (b). Curves 1 and 5 represent repumping by the FORT as described by $\Gamma_{sc}^{int}(\rho)$. Curves 2 and 6 show that energy can still be extracted when no spatial dependence of the repump scattering rate is employed, i.e. when $\Gamma_{sc} = 1$. When repumping is done with an additional repump laser, $\Gamma_{sc}^{det}(\rho)$ is used in the integral. Curve 4 is shown for $U_0(a) = -1$ mK, and curve 3 for $U_0(a) = -10$ mK.

Table 6.2: Repumping from the $|3, +2\rangle$ state. Tabulated are the percent probabilities that an atom decays from the excited state listed across the top to the ground state listed on the left side. These excited states are accessible with a $\Delta m = +1$ transition from the $|3, +2\rangle$ state. Based on calculations by Christopher J. Myatt.

	$5^2P_{3/2}$		$5^2P_{1/2}$
	$ 4', +3\rangle$	$ 3', +3\rangle$	$ 3', +3\rangle$
$ 3, +3\rangle$	25	42	33
$ 3, +2\rangle$	75	14	11
$ 2, +2\rangle$	0	44	55

The circular FORT is not as effective when repumping atoms from the $|2, +1\rangle$ state, where they are driven in the microwave cooling scheme. If the FORT is closest to the D_2 transition, an average over the appropriate Clebsch-Gordon probabilities indicates that only 15% of the repumping transitions return the atoms to the $|3, +3\rangle$ state to complete a closed cycle. 28% return the atoms to the $|2, 1\rangle$ state, and again no net cooling results. Unfortunately, 34% return to the shallowest $|2, +2\rangle$ state from which they are most likely lost before they can be pumped to the $|3, +3\rangle$ state.

In contrast, an additional circularly polarized repump laser tuned from the $5^2S_{1/2}$ $|2, +1\rangle$ to the $5^2P_{1/2}$ $|2', +2\rangle$ state should be much more efficient. As shown in Table 6.2, 56% of the repump transitions result in a closed cycle. For this additional laser to dominate the repumping process, the scattering rate of atoms in the $|2, +1\rangle$ state must be several times higher than the FORT. However, this will not cause significant additional heating because the vast majority of atoms are in the $|3, +3\rangle$ state where they are detuned several GHz from resonance with the additional repump laser.

6.2.3 Cooling Rates

Once the efficiency of the cooling process is understood, the maximum cooling rate is readily calculated. Because the Landau-Zener probability is very high at the turning points of the oscillation, after half an oscillation period no more atoms will be resonant with the drive frequency, because they will either be cooled or lost. Therefore, to continue cooling, the microwave or rf drive frequency must increase so as to interact with atoms of lower kinetic energy. As described in the previous subsection, the optimum rate at which to sweep the frequency ν is

$$\frac{d\nu}{dt} = \frac{4}{\tau_{\text{osc}}} \frac{\Omega_{\text{eff}}}{2\pi} \quad (6.6)$$

where τ_a^{osc} is the period of oscillation of atoms in the deeper of the two circular FORT potentials involved in the cooling cycle.

The maximum cooling rate is the ratio of the amount of energy carried away in one cooling event to the time between cooling events. As plotted in Fig. 6.4, the fraction (α) of energy removed in one cooling cycle depends on the initial energy E_i ;

$\Delta E = -\alpha E_i$. The time between events Δt , for a constant frequency sweep, also depends on the initial energy. The more energy an atom gives up in one cooling event, the longer it must wait before the drive frequency is resonant with its turning point again and it can experience another cooling cycle.

$$\Delta t = \frac{\Delta E}{h} \left(\frac{d\nu}{dt} \right)^{-1}.$$

The resulting cooling rate is surprisingly constant in time, independent of the atom's energy:

$$\frac{dE}{dt} = \frac{4\Omega_{eff}\hbar}{\tau_a^{osc}} \quad (6.7)$$

This calculation must break down when the time for an atom to be repumped (t_R) exceeds Δt above. In essence, that means that the atoms can no longer keep up with the sweep rate of the drive frequency. If t_R is limited by the time required for the atom to oscillate back to the center of the trap, then $t_R = 1/4\tau_b^{osc}$, where τ_b^{osc} is the period of oscillation in the shallow potential. Cooling then crosses into a different regime, in which the sweep rate is limited so that the atom is repumped before the drive comes into resonance with the frequency of the new turning point of the atom. This gives an exponentially decreasing cooling rate:

$$\frac{dE}{dt} = -\alpha E \frac{4}{\tau_b^{osc}} \quad (6.8)$$

and a resulting time-dependent energy of

$$E(t) = E_i e^{-4\alpha t / \tau_b^{osc}}. \quad (6.9)$$

For typical experimental parameters of $\Omega_{eff} = 2\pi \cdot 50$ kHz and $\tau_a^{osc} = 1$ ms, $dE/dt = 10$ mK/s. The energy (E_i) at which the expression for dE/dt changes from a constant to an energy-dependent expression is then $E_i = \Omega_{eff} \hbar \tau_b^{osc} / \alpha \tau_a^{osc}$. For the values above, $\tau_b^{osc} = 2$ ms, and $\alpha = 0.3$, $E_B/k_B = 17$ μ K.

6.2.4 Evaporative Cooling

Forced evaporative cooling is also a powerful technique that can be highly efficient in the limit of rapid collisions and long lifetimes. The speed with which the potential depth can be reduced and hence the cooling can be driven depends on the collision rate of the atoms. Because the circular FORT has much tighter confinement and higher collision rates, evaporation can proceed at much faster rates in this trap than in magnetic traps. For the best evaporative cooling configuration, one should operate the trap at a wavelength in which the $|b\rangle$ state is unbound. This is the case for $|2, 1\rangle$ state between 786 nm and 795 nm.

6.2.5 Heating Mechanisms

A variety of heating mechanisms can limit the performance of both Sisyphus and evaporative cooling. The heating due to collisions with background gasses is predicted by Beijerinck to be a modest $12 \mu\text{K/s}$ [17] in a 1 mK trap with a collisionally limited lifetime of 10 s.

Larger contributions come from simple photon scattering in the circular FORT. Even with perfect polarization, each photon absorbed on the cycling transition ($|3, +3 \rangle \rightarrow |4', +4 \rangle$) gives a recoil kick. The heating rate due to this process is a simple random walk in momentum space. The resulting heating rate is

$$\frac{dT}{dt} = \frac{\Gamma_{sc} v_R^2 m}{3 k_B}$$

where v_R is the recoil velocity (0.5 cm/s in Rb), m is the atomic mass, and k_B is Boltzmann's constant. Conveniently in Rb, for T in μK and v in cm/s, $m/k_B \approx 1$. Typical experimental parameters give 500 photons/s absorbed and spontaneously scattered from the FORT laser beam, and therefore a heating rate of $40 \mu\text{K/s}$.

The FORT atoms will also absorb photons from the Raman laser beams, and because these are not circularly polarized, they tend to randomize the m_F states. The resulting dipole force fluctuations can give rise to large heating rates, as shown in Chapt. 4, Fig. 4.7. In that chapter, an expression was derived for the exponential lifetime as a function of initial and final temperatures and the depths of the potentials involved. Using the same arguments, a heating rate can be directly derived. The resulting expression for energy as a function of time becomes:

$$E(t) = E_i e^{\frac{U_a}{U_b} \Gamma_h t} \quad (6.10)$$

where Γ_h is defined previously as the hopping rate between potentials. The resulting 1/e time constant is then $[\frac{U_a}{U_b} \Gamma_h]^{-1}$

For the Raman lasers detuned 0.4 nm, typical experimental parameters give 200 photon/s scattering rates and therefore $\Gamma_h \approx 10/\text{s}$. The derivative of Eq. 6.10 evaluated for an initial energy of 0.4 mK gives a large initial heating rate of 4 mK/s , nearly equal to the cooling rate.

Imperfect FORT polarization can still contribute to heating in the same way described in Chapt. 4. Therefore, the FORT laser polarization must be carefully controlled to keep the dipole force fluctuation heating from limiting the cooling.

Often, radiation trapping is cited as a limit to effective optical cooling schemes. This should not limit the performance of the schemes proposed here, because the FORT photons are very far from resonance, and therefore unlikely to be reabsorbed as they exit the atom cloud. Even the addition of a repump at 795 nm will not cause additional heating, because it is several GHz detuned from the majority of atoms in the trap.

6.2.6 Ultimate Temperatures

The limits of the optimized Sisyphus cooling process are found by examining the balance between the heating and cooling rates. The largest heating rate calculated

in the preceding section is caused by dipole force fluctuations induced by spontaneous scattering of photons from the Raman laser. However, this heating rate decreases with temperature, whereas the Sisyphus cooling rate is independent of temperature above about $20 \mu\text{K}$. Therefore, if the temperature is low enough to start the cooling process, this heating rate can only affect the Sisyphus cooling below the crossover temperature, where Sisyphus cooling starts to turn off. In that case, the differential equation that describes the competition between heating and cooling is simply

$$\frac{dE}{dt} = \left(-\alpha \frac{4}{\tau_b^{\text{osc}}} + \Gamma_h \frac{U_a}{U_b}\right)E.$$

For the parameters given in the previous section, the cooling term outweighs the heating by a factor of 15, and therefore this heating mechanism does not greatly impact the Sisyphus cooling rate.

Recoil heating due to FORT scattering of $40 \mu\text{K/s}$ does not limit the final temperature. Because this heating rate is independent of the atom's energy, and less than the constant cooling rate of 10 mK/s , this cannot limit the final temperature until the cooling turns off in the exponential regime. By setting the magnitudes of the cooling and heating rates equal to one another as above, the limiting temperature is 70 nK . Therefore, this heating rate will not limit the final temperature of the atoms, as this is far below the recoil limit of the cooling process. The constant heating rate due to background collisions of $12 \mu\text{K/s}$ should also not limit the final temperature, as that heating rate balances the cooling rate at an even lower temperature: 20 nK .

Finally, the cooling process itself causes some recoil heating, due to the spontaneous emission of photons in all directions. If a few repumping events are on average required to close the cooling cycle, the final temperature is about 250 nK . Thus the recoil limit seems to be the ultimate cooling limit of the Sisyphus process.

The above limits were established under the assumption of ideal repumping. If the cooling cycle is only 92% closed, then about 10% of the atoms are lost during each cooling event, and the number of atoms left after j cooling cycles will be 0.9^j . Thus to cool atoms a factor of 10 with $\alpha = 0.3$, cooling a factor of 10 results in a loss of 50% of the atoms. Even this loss should turn off as the atoms get colder, because atoms will no longer be lost from the very shallow $|2, +2\rangle$ state. Of course, as temperatures decrease, densities increase and therefore collisional losses will increase. Increased losses are not calculated in this document, but will undoubtedly be important.

6.2.7 Cooling with a Pulsed Drive

As mentioned on page 74, it may not be possible to drive transitions between $|a\rangle$ and $|b\rangle$ continuously due to the adiabatic interaction of the atoms with the drive frequency. In this case, a pulsed implementation similar to that used in gravitational Sisyphus cooling may be necessary. To do this in the circular FORT, the MOPA drive is turned on for about $1/4 \tau_a^{\text{osc}}$ in order to induce Rabi flopping between $|a\rangle$ and $|b\rangle$ that results in 50% of the population in each state. Then $1/4 \tau_a^{\text{osc}}$ later, if the repumping is induced by an additional laser, the repump laser should be turned on for an additional

$1/4 \tau_a^{\text{osc}}$. This cycle should then be repeated every $3/4 \tau_a^{\text{osc}}$ so that the drive can interact with atoms in every phase of oscillation. Therefore the optimum sweep rate is a factor of 3 slower than that given by Eq. (6.6) and therefore so is the optimum cooling rate [Eq. (6.7)] from 10 mK/s to 3 mK/s.

One of the heating rates scale with the time that the Raman laser beams illuminate the trapped sample, specifically the dipole force fluctuation heating induced by the spontaneous scattering of Raman laser light as described on pg. 82. The reduced duty cycle of the Raman lasers changes the heating from 4 mK/s to 1.3 mK/s. The other heating rates are not reduced with the Raman laser duty cycle. Therefore the temperatures at which the cooling and heating balance will increase by up to a factor of 3. Fortunately the final temperature appears to be limited by the recoil heating due to spontaneous emission during the cooling cycle, which remains the same as previously estimated.

6.3 Experimental Implementation

6.3.1 RF considerations

To implement the Sisyphus cooling scheme, we first explored the rf drive. We attempted to couple rf into the vacuum chamber by placing a drive coil about 2 in. dia. on a 6 in. flange (4 in. clear aperture window), and drove it at frequencies between 1 and 10 MHz. Unfortunately, the stainless steel vacuum chamber is an excellent shield of rf. To quantify that statement, we measured the voltage across a pick-up coil as a function of the distance between the pick-up coil and the source coil, in free space and in the presence of a 4 in. dia. pipe, mimicking our vacuum chamber. The results, shown in Fig. 6.5, indicate that the rf that reaches the atoms at about 16 cm from the coil is suppressed by 3 orders of magnitude in amplitude, and therefore 6 orders of magnitude in power. Consequently, we concluded that the only way to couple rf into our vacuum chamber is to break vacuum and insert a coil very close to the atoms.

6.3.2 MOPA

Rather than open the vacuum chamber, we chose to pursue the two-photon stimulated Raman transition option. This was made easier by the existence of a microwave-modulated master oscillator power amplifier MOPA system already constructed by Neil Claussen. A typical MOPA system [100] consists of a grating-tuned diode laser injected into a tapered amplifier. Multiple diode laser beams at different frequencies can also be injected into the amplifiers [101]. Our MOPA relies on microwave modulation [96] to create 2 frequencies in the master oscillator (MO) diode laser. The length of the cavity is chosen to be resonant with the modulation frequency, so that large modulation depths are achieved with small injected powers. Typically two frequency sidebands are created with powers up to about 50% of the power remaining in the carrier, and 25% of the initial power in each sideband.

The output from the MO is then tightly focused and mode-matched into the power amplifier (PA) that is driven at between 1.5 and 1.8 Amps. The output from the PA

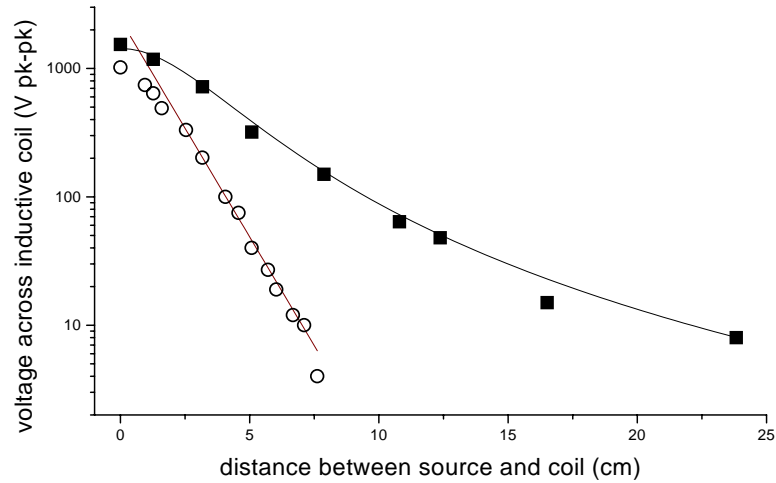


Figure 6.5: Demonstration of the difficulty of coupling rf (frequency = 3.7 MHz) radiation into a vacuum chamber from outside. In free space (■), the field detected by an inductive coil decreases as $1/r^3$. However, when the rf radiation must propagate along the axis of a metal cylinder (dia. = 4 in) (○), the field decays with a e^{-1} length of 1.3 cm.

contains all the frequency components from the MO. Unfortunately, as discussed in detail in Ref. [100], the output from the PA also contains a lot of broadband radiation spread over 20 - 30 nm. The power density of this radiation decreases by more than an order of magnitude when the MO is injected into the PA, making it about 1.5% of the power at the amplified frequency per 0.1 nm [100]. If the MOPA is focused to a total intensity of 1.5×10^5 mW/cm², the amount of intensity within a linewidth of the Rb resonance is about 3.4×10^{-4} mW/cm², resulting in a scattering rate of 2.5×10^3 photons per s, which is larger than the scattering due to the amplified power at the desired wavelength by a factor of 10 when the MO is tuned 0.5 nm from resonance. The effect of the scattering induced by the broad-band power emitted from the PA was clearly observable. The lifetime of FORT atoms in the presence of the MOPA light decreased from 7 s to 200 ms at MOPA total intensities as small as 10^4 mW/cm².

This broad-band radiation is difficult to filter out using conventional filters, because we want to block broadband radiation on resonance with the atoms, but completely pass the amplified power about 0.5 nm away. Typical interference filters do not have narrow enough bandpass widths or sharp enough cut-offs for this application. Fabry-Perot cavities might be made to work, but would require a lot of effort. Therefore, the most logical filter is an absorption cell of the appropriate species, in this case Rb. Therefore, a Rb cell was placed in the MOPA beam path and heated such that the coldest point in the cell is about 55°C, giving a vapor pressure of 6×10^{-6} Torr, 30 times that of room temperature. The effect of broadband MOPA light on the FORT

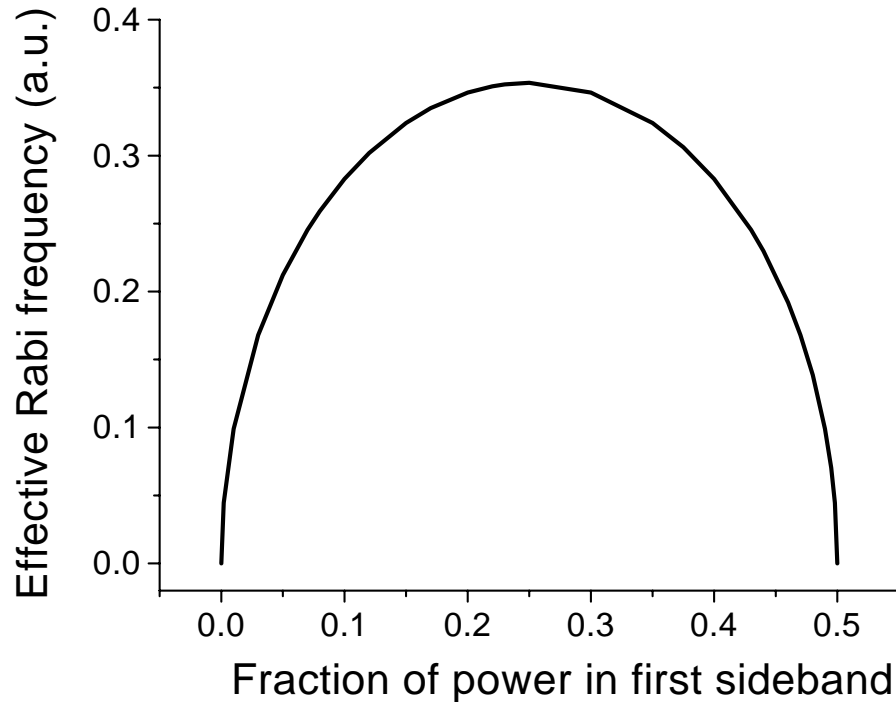


Figure 6.6: Calculated relative Rabi Frequency vs. the efficiency of MOPA modulation. The MOPA modulation is defined as the ratio of the power in one sideband over the power at the carrier frequency, assuming the power is equal between the +1 and -1 order modulation peaks.

lifetime became much less significant. Without any injected light, the lifetime of the atoms changes only about 10% when illuminated by the PA broadband radiation under conditions in which the maximum MOPA intensity is a total of 10^5 mW/cm².

The optimum modulation amplitude of the MOPA light in order to drive two-photon Raman transitions is readily calculated. Because both sidebands are equally populated, but the transition is driven by an interference between one sideband and the carrier, over-modulation can deplete the carrier and reduce the transition rate. Thus the optimum requires that half the power remain in the carrier and 25% in each sideband. However, it is not a steep function, so the requirements on modulation are not stringent, as shown in Fig.6.6.

6.3.3 Procedure

A schematic of the experiment is shown in Fig. 6.7. The procedure is very similar to that described in Chapter 4. Primary differences include the absence of a repump beam to help with loading. Also, we have the capability to image the atoms

as in Chapter 5. Thus we are able to measure the temperature of the atoms in ballistic expansion as the atoms are cooled with the MOPA laser beam. Finally, we include the MOPA laser, focused to 1.5×10^5 mW/cm², counterpropagating the FORT laser. This choice of geometry allows the highest intensities for driving the two-photon transitions, but only allows $\Delta m = -2$ transitions. Therefore state $|b\rangle$ in the cooling scheme must be $|2, +1\rangle$ because $|2, +2\rangle$ is inaccessible, although it would provide slightly higher values of α . Thus with an infinite intensity, directing the MOPA beams perpendicular to the FORT may be preferable. The MO is modulated at frequencies near 3035 MHz, as described above. We have the capability to trigger a ramp of that frequency, linear to within about 10%, with control over the ramp rate, duration, beginning and ending frequencies.

6.4 Preliminary results

6.4.1 Two-Photon Stimulated Raman Transitions

To verify that the MOPA laser could actually excite two-photon stimulated Raman transitions, we monitored the number of atoms stored in the FORT for a fixed FORT storage time while the MOPA illuminated the atoms for the majority of that time. The frequency of the modulation was changed from shot to shot, and the number remaining in the trap was monitored. The resulting loss is shown in Fig. 6.8. This plot presents many interesting features that give information about the internal states and kinetic energies of atoms in the FORT and the depth of the FORT. No transitions occur blue of the 3035 MHz Rb resonance, implying that no atoms are being driven to deeper potentials, only shallower ones. This is a weak indication of the spin-polarization we measured previously in Chapter 6. The depth of the potential can be measured by the shift of the steep edge. This occurs 35 MHz red of the Rb unshifted resonance, implying a 50 MHz AC stark shift at the bottom of the $|3, 3\rangle$ potential, or 2.5 mK. Calculated values for this trap are 1 mK, assuming $w_0 = 60 \mu\text{m}$. This value decreased the next day by 10 MHz, and these are the conditions under which the remaining data were taken.

6.4.2 Cooling with Stationary Frequency

Figure 6.9 shows observed temperature as a function of time, for the frequency fixed at a detuning of 22.5 MHz below the Rb resonance. During the cooling, the number of atoms in the FORT decreased between a factor of 20 and 50. The uncertainty arises because the peak optical depth after expansion is monitored, but not the total number. The conversion of the peak optical depth relies on knowledge of the scaling of the length of the FORT. In (b), \blacksquare are calculated assuming the longitudinal dimension does not contract and is therefore not in thermal equilibrium with the other dimensions, while \circ show N assuming thermal equilibrium in all 3 dimensions. Finally, phase space density is computed assuming the sample is in thermal equilibrium, and is seen to increase by a factor of about 15.

The mechanism here is most likely primarily evaporative. Because the frequency is not changing with time, most atoms are not excited at the turning point of their

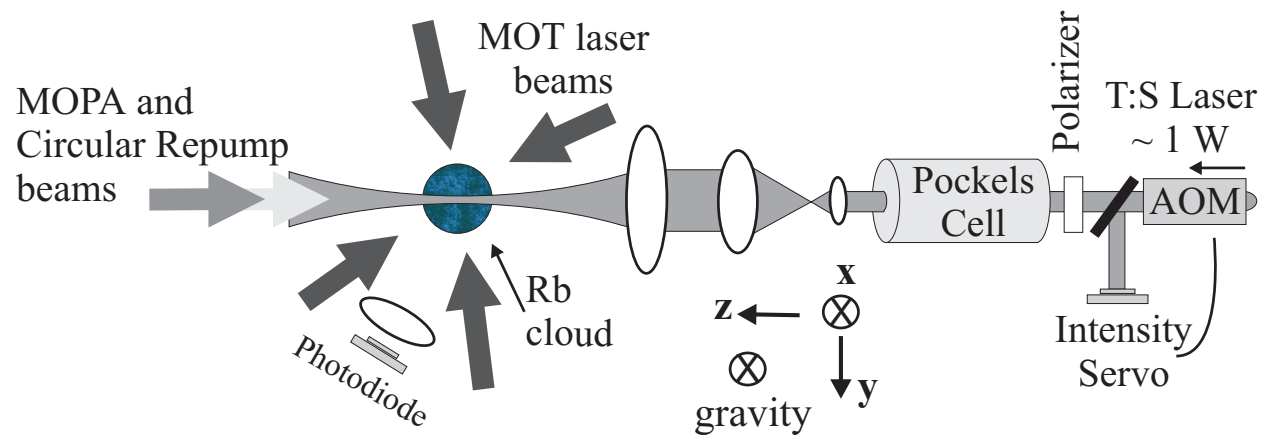


Figure 6.7: Layout of the all-optical two-photon stimulated Raman cooling scheme. Primary differences between this and Fig. 4.4 include the addition of a MOPA laser beam counter-propagating the FORT. The additional repump shown to counter-propagate the FORT laser beam is only proposed, and has not yet been implemented.

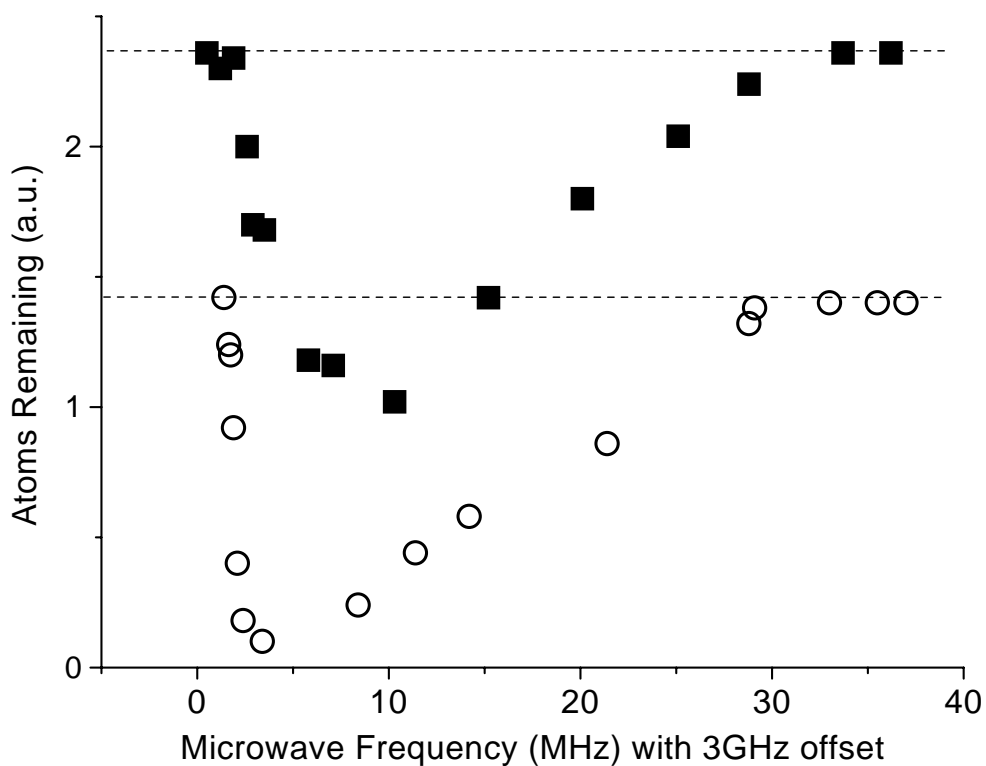


Figure 6.8: Loss from the circular FORT due to ground-state changing transitions as a function of the microwave frequency driving the transition. The resonance frequency for atoms in free space is 3035 MHz. (■) represent a FORT storage time of 250 ms and a cooling duration of 150 ms, while (○) show the same data for a longer FORT storage time (500 ms) and a longer cooling duration of 480 ms. Because at longer times the signal drops all the way to zero, the shape of the curve is distorted and the slope of the curve near the bottom of the trap goes to zero.

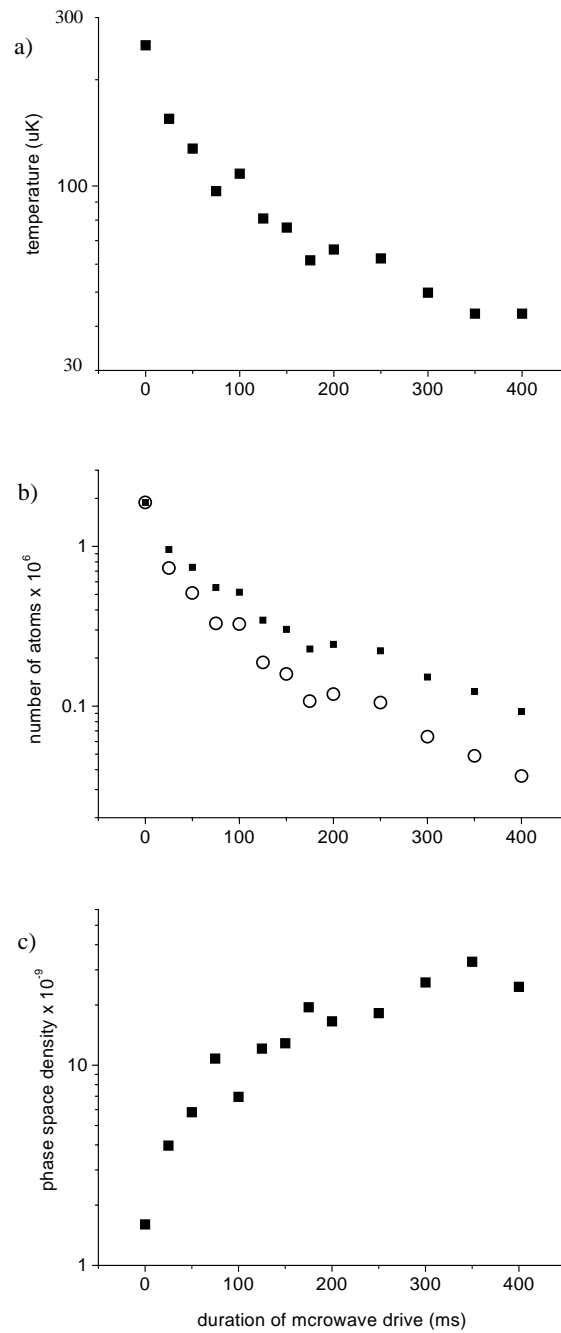


Figure 6.9: While the microwave drive frequency was held fixed at 3012.5 MHz, the time during which it was applied was varied simultaneously with the FORT storage time. (a) Shows the change in temperature, (b) number, and (c) the deduced phase space density, assuming the cloud remains in thermal equilibrium. In b), (■)'s represent the number left assuming the longitudinal dimension of the trapped sample does not change and (○)'s represent the number assuming all dimensions are in thermal equilibrium.

oscillation. Instead they are excited to state $|b\rangle$ with large kinetic energies, from which they are lost. However, at very low temperatures, this mechanism must turn off because all states in the circular FORT are trapped (ie. $U_0 < 0$). Perhaps this is the cause of the turnoff in cooling, along with substantial number loss.

6.4.3 Cooling with Swept Microwave Frequency

Once two-photon Raman transitions were demonstrated and cooling was demonstrated at a fixed frequency, cooling with a swept drive frequency was demonstrated. The frequency ramp began at the unshifted resonance of the ground-state splitting, and was swept at a constant rate for a variable time. Therefore the duration of the sweep also represents a “deeper cut” into the cloud, or allows interactions with increasingly colder atoms. The results are shown in Fig. 6.10. Phase space density increases by a factor of 5. In addition, the number loss is about a factor of 7.5, which could be ascribed to inefficient evaporation. At the lowest temperatures, however, evaporation seems unlikely because all states in the circular FORT are trapped at this wavelength. Thus additional losses are again likely to be due to collisional losses caused by increased density.

A comparison of the cooling results is at first glance perplexing. The fixed frequency data gives lower temperatures ($30\ \mu\text{K}$ vs. $80\ \mu\text{K}$), and higher phase space density increase (factor of 10 vs. factor of 5). Even in reaching $80\ \mu\text{K}$, the fixed frequency cooling gave comparable number loss and slightly higher (factor of 1.5) phase space density increase. Perhaps the fixed frequency cooling is initiating an evaporative cooling mechanism, while the swept frequency is poorly optimized for Sisyphus cooling. In both cases, the Sisyphus cooling may be turning off as the atoms get colder and the Landau-Zener transitions become increasingly adiabatic. Further study is warranted.

6.4.4 Heating Rates

Once cooling is shown to work, heating rates are easily measured by applying a cooling pulse and then watching the trapped sample heat up with time. As shown in Fig. 6.11, rates of $150\ \mu\text{K/s}$ are measured in the circular FORT in the absence of any additional laser light. This rate is consistent with a 5-10 s lifetime in a 1 mK trap. The expected heating rate in this trap, calculated earlier, is only $46\ \mu\text{K/s}$. However, the FORT polarization is not likely to be perfectly circular, and additional dipole force fluctuation heating, in conjunction with the heating already described, can easily cause the higher measured rate.

6.5 Conclusion

Sisyphus cooling and forced evaporative cooling schemes are theoretically very powerful cooling mechanisms in the circular FORT. Sisyphus cooling rates of up to $10\ \text{mK/s}$ are possible, and limiting temperatures approaching the recoil limit may be possible. Initial results show that the temperature can be reduced by a factor of 4 to $80\ \mu\text{K}$ while the number decreases by only a factor of between 2 and 6. Significant

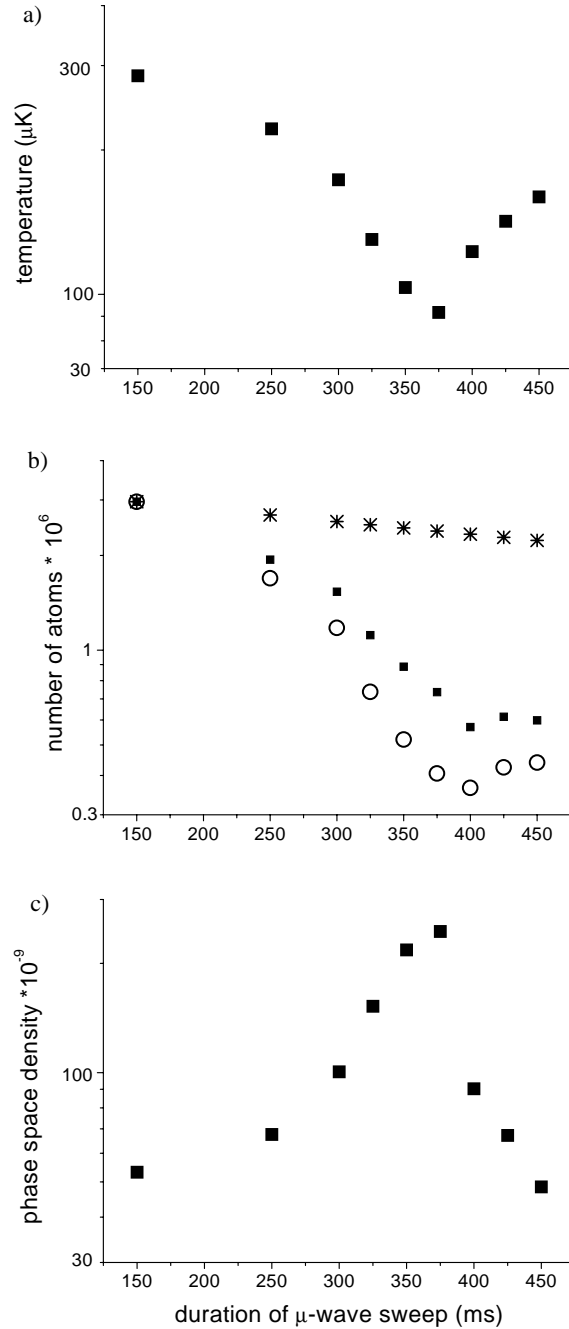


Figure 6.10: Atoms in the FORT are continually illuminated by the Raman beams while the microwave frequency was swept at a constant rate, starting from the unshifted resonance of 3035 MHz. As time increases, the end point of the sweep changes, effectively cutting deeper into the cloud. 150ms corresponds to a sweep of 9.8 MHz. Plotted are (a) the temperature of the atoms after cooling, (b) the number of atoms remaining after cooling, and (c) the resulting phase space density, assuming the sample is in thermal equilibrium. In b), (■)'s represent the number left assuming the longitudinal dimension of the trapped sample does not change, (○)'s represent the number assuming all dimensions are in thermal equilibrium, and finally the (*)'s show the time-dependence of atoms in the FORT during that time without any cooling.

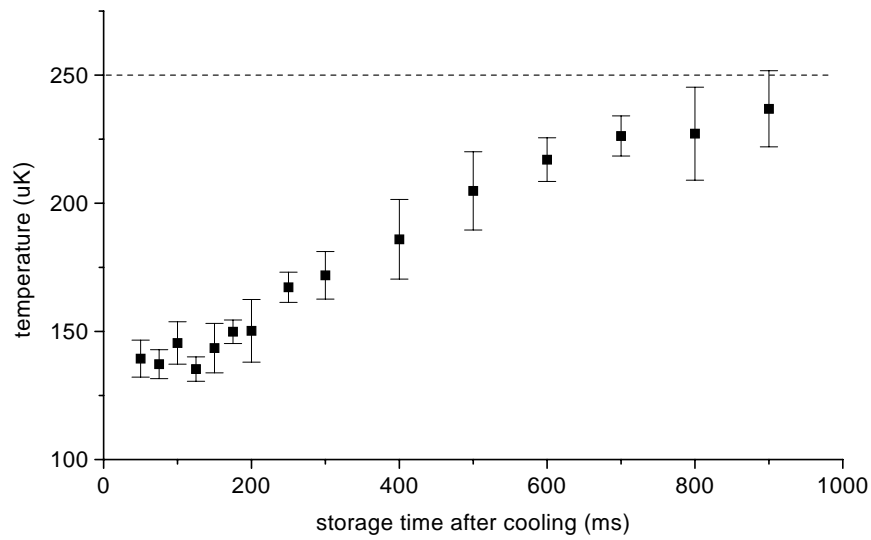


Figure 6.11: Heating rate of atoms stored in the circular FORT. Temperature is plotted as a function of time the atoms are stored in the FORT after a 50 ms cooling pulse is applied.

improvements in the Sisyphus contribution to this cooling scheme may be realized by utilizing an additional circularly polarized repump on the D_1 line, tailoring the frequency sweep to coincide with the optimum cooling rate, and pulsing the the MOPA on and off rapidly. Evaporation has not been optimized, and most likely the evaporative cooling effects could be improved significantly by tailoring the evaporation sweep rate as is done in magnetic traps. [67]